A generalized reactive force field for nonlinear hydrogen bonds: Hydrogen dynamics and transfer in malonaldehyde

Yonggang Yang and Markus Meuwly

Citation: The Journal of Chemical Physics **133**, 064503 (2010); doi: 10.1063/1.3447701

View online: http://dx.doi.org/10.1063/1.3447701

View Table of Contents: http://scitation.aip.org/content/aip/journal/jcp/133/6?ver=pdfcov

Published by the AIP Publishing

A generalized reactive force field for nonlinear hydrogen bonds: Hydrogen dynamics and transfer in malonaldehyde

Yonggang Yang and Markus Meuwly[a)]
Department of Chemistry, University of Basel, Klingelbergstrasse 80, 4056 Basel, Switzerland

(Received 1 December 2009; accepted 18 May 2010; published online 9 August 2010)

Using molecular dynamics (MD) simulations, the spectroscopy and dynamics of malonaldehyde is investigated. To this end, the recently proposed molecular mechanics with proton transfer (MMPT) potential is generalized to nonlinear hydrogen bonds. The calculated properties for malonaldehyde in both gas and condensed phases, including equilibrium geometries, infrared spectra, tunneling splittings, and hydrogen transfer rates, compare well with previous experimental and computational works. In particular, by using a harmonic bath averaged (HBA) Hamiltonian, which is based on a reaction path Hamiltonian, it is possible to estimate the tunneling splitting in an efficient manner. It is found that a zero point corrected barrier of 6.7 kcal/mol and effective masses of 1.234 (i.e., 23.4% larger than the mass of a physical H-atom) and 1.117 (for the physical D-atom) are consistent with the measured splittings of 21.6 and 2.9 cm^{-1}, respectively. The HBA Hamiltonian also yields a pair of hydrogen transfer fundamentals at 1573 and 1267 cm^{-1}, similar to results obtained with a reaction surface Hamiltonian on a MP2/6-31G** potential energy surface. This amounts to a substantial redshift of more than 1000 cm^{-1} which can be rationalized by comparison with weakly (HCO^+: rare gas) and strongly ($H_2O—H^+—OH_2$) proton-bound systems. Hydrogen transfer rates in vacuum and water were determined from the validated MMPT potential and it is found that the solvent enhances the rate by a factor of 5 at 300 K. The rates of 2.4/ns and 10/ns are commensurate with previous density functional tight binding *ab initio* MD studies. © *2010 American Institute of Physics*. [doi:10.1063/1.3447701]

I. INTRODUCTION

Proton transfer (PT) and hydrogen transfer (HT) reactions are of fundamental importance for various processes in chemistry and biology. Although the famous Grotthuss shuttling mechanism[1] was introduced more than 200 years ago, essential progress has only been achieved recently with modern spectroscopic techniques and high performance computer simulations.[2] From the experimental point of view infrared studies[3–5] were shown to be useful for probing the vibrational dynamics of hydrogen bonds. However, it should be noted that a complete assignment/interpretation of the spectra is difficult and greatly assisted by computational methods. In general, theoretical studies of systems with strong hydrogen bonds require quantum dynamics[6–9] while for weak hydrogen bonds, classical molecular dynamics (MD) is sufficient.[10,11] It has been shown very recently[12,13] that suitably modified empirical force fields together with MD simulations can also capture features of strong hydrogen bonds if reactive force fields are used. However, to study more general cases of proton and hydrogen transfer reactions additional modifications and generalizations of the force field are required.

Among various hydrogen bonded systems which are of current interest, malonaldehyde (MA) has been one of the most extensively studied ones to elucidate the characteristics of intramolecular HT processes. Figure 1 shows the *enol* form of MA together with the transition state for HT. A large ground state splitting of 21.583 cm^{-1} has been observed by different experiments with very high precision.[14,15] Such a splitting suggests rapid HT (with lifetime of picosecond time scale). Apart from the splitting, intensive experimental work on the infrared spectrum has also been performed.[16–20] Early experiments have measured the gas phase infrared spectrum of MA at room temperature.[16,17] The observed band at around 1600 cm^{-1} has been assigned to the C═O stretch fundamental and another band close to 2900 cm^{-1} has been assigned to the O—H^* stretch fundamental, where H^* refers to the transferring hydrogen atom. Low temperature measurements of the spectra of MA isolated in rare gas matrices have also been carried out and compared to *ab initio* calculations at the MP2/DZP level.[18,19] A recent experiment with high spectral resolution has provided more details about the couplings of the C═O stretch with rotations.[20]

From a theoretical perspective, it is quite challenging to assign the spectrum of a fairly strong hydrogen bond due to the substantial coupling between the hydrogen motion and other degrees of freedom.[7,21] To go beyond the approximations used in normal mode analysis, e.g., in *ab initio* calculations, quantum dynamics has been used to more realistically describe, in particular, the O—H^* stretch fundamental in MA.[22–26] A recent vibrational-self-consistent-field dynamics on a truncated (second order) correlation expansion of MP2/6-31G** potential[22] leads to a reduction of the O—H^* stretch fundamental frequency by about 500 cm^{-1} compared to the harmonic one and gives good agreement with the ex-

[a)]Electronic mail: m.meuwly@unibas.ch.

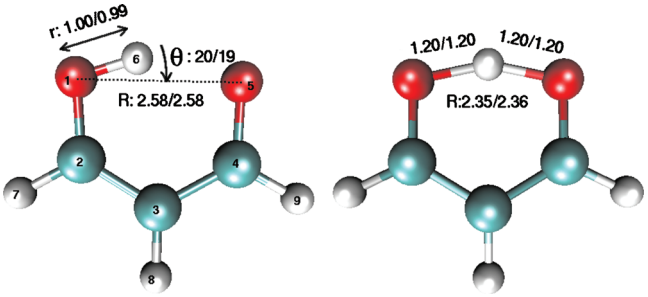

FIG. 1. Minimum and transition state geometries of MA with bond lengths (in Å) and angles (in degrees) obtained from *ab initio* and CHARMM/MMPT optimizations, respectively.

perimental one at around 2900 cm^{-1}. More accurate full-dimensional quantum dynamics investigations on truncated potentials[23–26] have also been performed very recently. The O—H^* stretch fundamental has been studied in Ref. 23 using a reaction surface Hamiltonian (RSH) with a MP2/6-31G** potential including up to sixth order couplings of two reaction surface coordinates and the remaining $3N-8$ normal coordinates. This gives an O—H^* stretch fundamental frequency at 1672 cm^{-1} (1693 cm^{-1} with an isolated two dimensional model) and the authors suggest that the previous assignment of the O—H^* stretch fundamental to around 2900 cm^{-1} is probably incorrect. Concerning the ground state tunneling splitting, Ref. 23 has reported a value of 11 cm^{-1} while the other three investigations[24–26] have obtained splittings, which agree with the experiment quite well. In particular, Ref. 25 has reported the splitting of 21.6 cm^{-1} (normal coordinate representation) and 22.6 cm^{-1} (Cartesian coordinate representation) using a CCSD(T) potential with correlations up to seventh order. In the most recent work[26] the transferring proton is treated at the same level as the electrons that gives a splitting of 24.5 cm^{-1} even only with a MP2 potential expanded up to second order of heavy atom coordinates. However to increase the accuracy in Ref. 26 more diabatic potential energy surfaces (PESs) have to be included. As can be seen all the converged full-dimensional quantum dynamics mentioned above are extremely computationally expensive.

In the present work a recently developed, efficient method to treat PT together with empirical force fields [molecular mechanics with proton transfer[13] (MMPT)] will be generalized to nonlinear proton-bound motifs. The detailed description of the modified MMPT potential applicable to both linear and nonlinear hydrogen bonds will be introduced in Sec. II A. The PES is validated by calculating infrared spectra of MA and its isotopomers in vacuum from normal mode analysis and explicit long time MD simulations (see Sec. III B). Next, a newly developed harmonic bath averaged (HBA) Hamiltonian method will be discussed in Sec. III C, with which the ground state tunneling splitting is obtained with surprisingly small computational effort. Apart from the spectra and splitting, HT rates in both vacuum and solution are also investigated. The conclusions of present work are summarized in Sec. IV.

II. METHODS

A. Modified MMPT potential

MMPT was developed as an efficient method to study PT and HT on a qualitatively (topologically) correct, fully dimensional PES for predominately linear hydrogen bonds. Here, the PES will be generalized to nonlinear hydrogen bonds such as the intramolecular hydrogen bond in MA. In the following R and r denote the D-A and D-H distances of a D-H···A hydrogen bond motif and the angle between $\vec{r}$ (D-H) and $\vec{R}$ (D-A) is θ, as shown in Fig. 1 for MA. For further considerations symmetric hydrogen bonds are assumed in which donor D and acceptor A are identical. The generalization to asymmetric hydrogen bonds with D different from A is straightforward and given below. For numerical convenience it is advantageous to define a dimensionless coordinate ρ,

$$\rho = (r\cos\theta - r_{\min})/(R - 2r_{\min}),$$

where $r_{\min}=0.8$ Å is an arbitrary but sufficiently small D-H separation.[13] For a linear hydrogen bond the above definition is identical to the original MMPT potential,[13] whereas for a nonlinear hydrogen bond the present definition is better suited. In the following it is advantageous to define a perpendicular bending displacement $d=r\sin\theta$ instead of θ. In terms of the set of coordinates $\{R,\rho,d\}$ it is straightforward to express the symmetry of the potential of a symmetric hydrogen bond as

$$V_{\mathrm{PT}}(R,\rho,d) = V_{\mathrm{PT}}(R,1-\rho,d). \tag{1}$$

In general, the coupling between d and $\{R,\rho\}$ is less significant than the one between R and ρ. Therefore it is natural to use an $\{R,\rho\}$-dependent "adiabatic" one-dimensional potential V_d. The following expression gives the correct symmetries for both linear and nonlinear hydrogen bonds:

$$V_{\mathrm{PT}}(R,\rho,d) = V_0(R,\rho) + V_d(R,\rho,d), \tag{2}$$

where $V_0(R,\rho)$ is the isotropic potential parametrized as follows:[13]

$$\begin{aligned} V_0(R,\rho) = {} & D_{\mathrm{eq}}(R)[1-\exp(-\beta(R)(\rho-\rho_{\mathrm{eq}}(R)))]^2 \\ & + D_{\mathrm{eq}}(R)[1-\exp(-\beta(R)(1-\rho-\rho_{\mathrm{eq}}(R)))]^2 \\ & - D_{\mathrm{eq}}(R) + c \end{aligned}$$

and $V_d(R,\rho,d)$ is an $\{R,\rho\}$-dependent harmonic potential

$$V_d(R,\rho,d) = \tfrac{1}{2}k(R,\rho)[d - d_e(R,\rho)]^2 \tag{3}$$

for the perpendicular bending degree of freedom, where the force constant $k(R,\rho)$ and the equilibrium bending displacement $d_e(R,\rho)$ have the same symmetry as mentioned in Eq. (1). It is also straightforward to generalize Eq. (3) to an anharmonic potential if necessary.

In the following Eq. (2) will be used to investigate MA which exhibits a nonlinear hydrogen bond. The explicit $\{R,\rho\}$-dependence of V_d is

$$k(R,\rho) = k_{TS} + \xi[V_0(R,\rho) - V_0^{TS}],$$
$$d_e(R,\rho) = d_e(\rho) = d_e^{TS} + \eta(\rho - \rho_{TS})^2, \quad (4)$$

where the coefficients ξ and η are given by $\xi=(k_{min}-k_{TS})/(V_0^{min}-V_0^{TS})$ and $\eta=(d_e^{min}-d_e^{TS})/(\rho_{min}-\rho_{TS})^2$, respectively. Here, "min" and "TS" denote values at minimum and transition state (TS) configurations, respectively. It is straightforward to generalize Eq. (4) to asymmetric hydrogen bonds (where D differs from A) where a suitably defined midpoint reference configuration can be used if no transition state configuration is available.

Eq. (2) contains 14 parameters $(p_1,\ldots,p_{14})$ that need to be parametrized in an appropriate way. The parameters $p_1,\ldots,p_9$ are related to $D_{eq}(R)$, $\beta(R)$, and $\rho_{eq}(R)$ of a Morse potential and p_{11} is related to the stabilization energy of the model compound.[13] The ten parameters have been obtained by applying three morphing transformations to the reported symmetric double minimum potential in Ref. 13 to rescale the energy V_{PT}, coordinate R, and coordinate ρ for MA. The remaining four parameters are

$$p_{10} = \xi,$$
$$p_{12} = k_{TS} - \xi V_0^{TS},$$
$$p_{13} = \eta,$$
$$p_{14} = d_e^{TS},$$

which can be obtained from fits around the minimum and transition state configurations to *ab initio* calculations. The same implementation for the asymmetric case contains 30 parameters. The parameters $p_1,\ldots,p_{26}$ are the same as detailed in Ref. 13 except that a new definition for ρ is used. The last four parameters are defined in a similar way as the above four parameters for the symmetric cases. For the present application to MA only a parametrization for the symmetric case is required and pursued further.

To obtain initial parameters for the PES that properly describe the stationary configurations of MA, one-dimensional relaxed potential energy scans along the bending coordinate d were carried out around the minimum and transition state configurations with the GAUSSIAN03 suite of programs.[27] The fitted force constants and equilibrium displacements are

$$k_{min} = 80.217 \text{ kcal/mol/Å}^2, \quad d_e^{min} = 0.343 \text{ Å},$$

and

$$k_{TS} = 141.338 \text{ kcal/mol/Å}^2, \quad d_e^{TS} = 0.220 \text{ Å},$$

respectively. The calculated HT barrier height at the CCSD(T)/6-311++G** level with the MP2 geometries is $\Delta E_b=4.36$ kcal/mol from which the remaining two parameters in Eq. (4) are obtained,

$$\xi = 14.028 \text{ Å}^{-2}, \quad \eta = 0.963 \text{ Å}^{-1}.$$

To adapt this PES to other chemical environments, morphing transformations can be used.[28,29]

B. MD simulations

All MD simulations are carried out with the CHARMM program[30] together with provision for the modified MMPT potential. The MA structure was initially optimized at the MP2/6-311++G** level using the GAUSSIAN03 suite of programs, which was also used for all subsequent *ab initio* calculations.[27] Starting from this structure the system is gradually heated to 300 K followed by a 1 ns equilibration with a time step of 0.2 fs. The final production run is a 10 ns free dynamics with a time step 0.1 fs corresponding to a microcanonical (*NVE*) ensemble. For the dynamics in solution, MA is solvated in a pre-equilibrated TIP3P (Ref. 31) water box with size of $16\times25\times25$ Å^3. MD simulations were carried out with periodic boundary conditions and a similar heating, equilibration (1 ns), and production (10 ns) protocol was followed except that the time step is 1.0 fs. All bonds involving hydrogen atoms in the solvent were kept fixed by using SHAKE.[32] For the long range interactions the electrostatic interactions are cut off at 14 Å with shift truncation and the van der Waals interactions are switched off by switch scheme with a switch region from 10 to 12 Å.[33] Average fluctuations around the average energy E in the *NVE* simulations is $\delta E=0.0003$ kcal/mol for simulations in vacuum and $\delta E=0.2$ kcal/mol in solution.

The infrared spectrum is calculated from the Fourier transform of the dipole-dipole autocorrelation function $C_\mu(t)$ with μ being the dipole moment. The absorption line shape can be obtained from[34,35]

$$I(\omega) = \omega(1 - e^{-\hbar\omega/k_BT}) \int_0^\infty C_\mu(\tau) e^{-i\omega\tau} d\tau,$$
$$C_\mu(\tau) = \langle \mu(t_0)\mu(t_0+\tau)\rangle_{t_0}.$$

Here, $\langle\cdots\rangle_{t_0}$ denotes averaging over all the time t_0. A thermal prefactor which reflects the occupation of the vibrational energy levels has been included with k_B being the Boltzmann constant and T the temperature in Kelvin. Numerically the autocorrelation function is transformed using a fast Fourier transform with a Blackman filter to minimize noise.[36]

To obtain HT rates the D-H and H···A distances are analyzed by means of Hazard plots.[37] For this, the n transition times $t_1,t_2,\ldots,t_n$ are arranged in ascending order and plotted against the expectation values of the corresponding cumulative hazards (see below). A transition has occurred when the D-H (or H-A) bond is broken and the H-A (D-H) bond is formed at a particular time step along the trajectory. The hydrogen atom is considered to be bonded to D (or A) when the D-H (or H-A) distance is smaller than a certain cutoff $r_c=1.2$ Å. It has been previously shown[10,13] that different values of r_c do not appreciably affect computed transfer rates. The expectation of the cumulative hazard at the time of the kth transition is defined by $H_k=\Sigma_{i=0}^{k-1}[1/(n-i)]$. Straight lines in hazard plots indicate a Poisson process, i.e., the probability of the occurrence of an event is independent of the past history. The reaction rate of the process is then given by the slope of the hazard plot.[37]

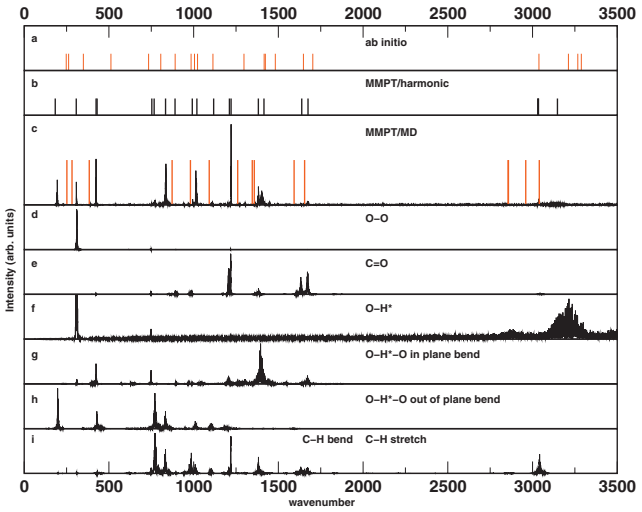

FIG. 2. Calculated infrared spectrum of MA in vacuum and assignments. Panels (a) and (b) show a stick spectrum (no intensities) of harmonic frequencies from *ab initio* and CHARMM/MMPT normal mode analysis. Panel (c) is the infrared spectrum $I(\omega)$ (see text) from MD simulations and the wavenumbers of the experimentally observed lines as a stick spectrum. The following panels show power spectra (calculated from the Fourier transform of the autocorrelation function of the corresponding coordinate) of stretching vibrations [(d)–(f)], O—H*—O bending vibrations [(g) and (h)], and C—H bend and stretch vibrations (i).

III. RESULTS

A. Equilibrium properties of MA

Figure 1 shows the minimum and transition state configurations of MA in its electronic ground state. Taking the *ab initio* configurations as a reference, the parameters for the MMPT potential are fitted [Eqs. (2)–(4), see Sec. II A]. The remaining force field parameters are obtained from existing CHARMM parameters.[38] The full set of parameters that is used for the remainder of this work is summarized in the supplementary material.[39] The bond lengths and angles of minimum and transition states optimized by CHARMM/MMPT and MP2/6-311++G** are shown in Fig. 1. In particular, the large change in the O···O distance between the minimum and the TS structure is correctly captured and suggests a significant change in the potential curve for hydrogen motion along the HT coordinate.

B. Infrared spectra of MA and its deuterated isotopomers

Infrared spectra from the Hessian and from the MD simulations are calculated to validate the PES (through comparison with experiment) and to make approximate assignments of the spectral features. It should be noted that the main interest in the present work is to generalize MMPT to nonlinear H-bonds and not the development of a spectroscopically accurate, fully dimensional PES for MA. For the latter a recently developed procedure could be used.[40] To be consistent with previous investigations[22] the same numbering scheme $C_4H_9O_5$—C_3H_8=C_2H_7—O_1H_6 is adopted to label the atoms in Fig. 1. Harmonic frequencies from *ab initio* calculations and the MMPT force field are graphically shown in Figs 2(a) and 2(b) and Table I reports anharmonic spectra from MD simulations and experiment of MA (CHO—CH=CH—OH) and its deuterated isotopomers (CHO—CD=CH—OD and CDO—CH=CD—OH). Also, Fig. 2 shows the IR spectrum of MA from extensive MD simulations (10 ns) together with power spectra of particularly relevant internal coordinates. Each power spectrum is calculated from the Fourier transform of the autocorrelation function of the corresponding coordinate, which characterizes the mode of interest. These spectra are discussed in the following.

TABLE I. Assignments of the calculated infrared spectra of MA and its deuterated isotopomers. Also shown are the experimentally measured infrared spectra of the three isotopomers (Ref. 17) for comparison. The RMSDs (in cm^{-1}) between the simulated and experimental spectra (excluding the O—H* stretch) are reported in the last row. Assignments are made based on the power spectra as well as the isotope effects. See the text for more details. The last column refers to the spectral features labeled in Figs. 3 and 4 (abbreviations: simulated spectra—Sim., experimental date—Expt., and no data available from previous investigations—n.a.).

CHOCHCHOH		CHOCDCHOD		CDOCHCDOH		Assignment	
Sim.	Expt.	Sim.	Expt.	Sim.	Expt.	Mode	Figs. 3 and 4
200	252	200	n.a.	200	n.a.	Ring out of plane	
310	282	310	n.a.	310	n.a.	O···O stretch	
420	384	420	n.a.	420	n.a.	Ring out of plane	
740	873	630	582	675	754	O—H*—O out plane+C—H out plane	
840	981	750	670	775	766	O—H*—O out plane+C—H out plane	a
1010	1092	1010	1010	1010	964	O—H*—O out plane+C—H out plane	b
1220	1260	1220	1220	880	896	C—H_7+C—H_9 in plane (symmetric)	c
1390	1358	1320	1363	1340	1390	C—H_7+C—H_9 in plane (asymmetric)	
1410	1346	1060	1085	1380	1390	O—H*—O in plane	d
1620	1593	1610	1534	1580	1568	C=O asymmetric stretch	
1670	1655	1650	1655	1625	1645	C=O symmetric stretch	e
3040	2858	3040	2855	2250	2134	C—H/C—D stretch	
3040	2960	3040	2960	2250	2152	C—H/C—D stretch	
3040	3040	2250	2230	3040	3060	C—H/C—D stretch	f
3150	2856	2320	2140	3170	3170	O—H* stretch	g
83	···	73	···	57	···	RMSD of Sim. with respect to Expt.	

The fundamentals can be approximately assigned based on normal mode analysis, the power spectra corresponding to particular coordinates, and isotope effects (see Table I). It should be noted that due to the different couplings between the modes around the minimum and away from it, assignments based on the different approaches may vary. Furthermore, the anharmonicity along the HT motif and described in the MMPT potential may lead to additional changes between assignments from normal modes and the power spectra, respectively. Under such circumstances, assignments from the power spectra can provide a more robust and meaningful assignment than normal mode analysis. Assignments of all the bands from MD simulations of the three isotopomers are presented in Table I and compared to experimental data from Ref. 17. For most bands individual deviations less than 50 cm^{-1} are found between the experimental and calculated data. Such deviations are sufficient for approximate assignments of the bands but improvements to the force field are clearly possible, e.g., by using more refined morphing procedures or a more complete optimization of the force field.[40]

In the following, individual bands and their assignments are discussed based on the power spectra and isotopic shifts for MA and the isotopomers, and compared to experimental data. Figure 2(c) shows the calculated infrared spectrum from the MD simulations and experimental spectrum (red). Below 500 cm^{-1} three peaks are found which agree with experiment[17] and previous calculations.[22] At 310 cm^{-1} the O···O stretch can be identified from the corresponding power spectrum [Fig. 2(d)]. The other two lines at 200 and 420 cm^{-1} are ring deformations according to previous investigations.[22] The three modes almost do not shift upon deuteration which is expected for low frequency modes not involving hydrogen motion. The modes around 1000 cm^{-1} include contributions from the O—H*—O out-of-plane bending motion and different combinations of the three out-of-plane C—H bending motions, which form the most intricately entangled region. The complexity can also be seen from the power spectrum for the O—H*—O out-of-plane bending [see Fig. 2(h)]. At 1220 cm^{-1} a signal due to the C—H_7 and C—H_9 in plane bending is found which agrees well with the experimental value of 1260 cm^{-1}. The assignment follows from the power spectrum [Fig. 2(i)] as well as the fact that the band shifts down to 880 cm^{-1} for the CDO—CH=CD—OH isotopomer (green lines in Fig. 3). Note that Fig. 2(i) actually contains power spectra of all possible combinations of the stretching and bending vibrations of the three C—H bonds. The band at 1380 cm^{-1} is the O—H*—O in plane bending which also agrees well with the experimental value at 1346 cm^{-1}.[17] The power spectrum for this mode is shown in Fig. 2(g). For the deuterated isotopomer CHO—CD=CH—OD this band shifts down to 1055 cm^{-1} (red lines in Fig. 3), which again well reproduces the experimental value at 1085 cm^{-1}.[17] Then the experimentally observed C=O stretch doublet at around 1600 cm^{-1} can be identified. The calculated excitation frequencies for the C=O stretch doublet are 1570 and 1620 cm^{-1}, which agree well with the experimental ones at 1593 and 1655 cm^{-1}. To identify this mode more clearly one can refer to the corresponding power spectrum in Fig. 2(e). It

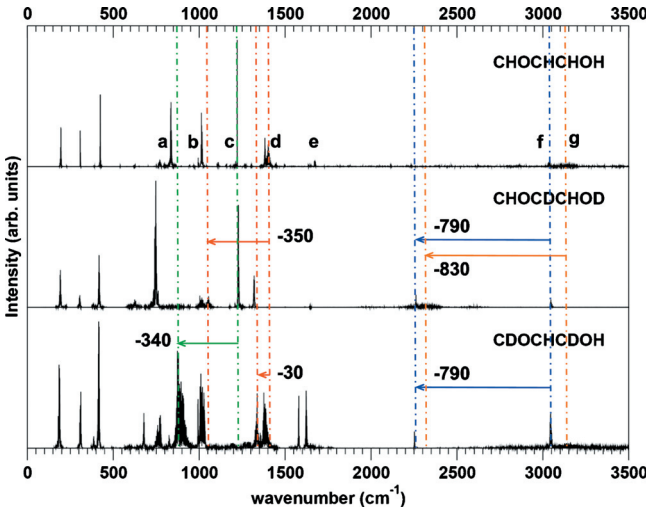

FIG. 3. Infrared spectra of MA and its deuterated isotopomers in vacuum. From top to bottom are CHO—CH=CH—OH, CHO—CD=CH—OD, and CDO—CH=CD—OH, respectively. The orange, blue, red, and green lines correspond to the O—H* stretch, C—H stretch, O—H*—O in plane bending, and C—H_7+C—H_9 in plane bending, respectively. Bands of particular interest are labeled (a)–(g) with detailed assignments in Table I.

is expected that slight adjustments of the C=O force constant will lead to even more quantitative agreement which is not further pursued here. Finally, there are high frequency bond stretching vibrations. The nearly threefold degenerate C—H bond stretch is at 3040 cm^{-1} and the O—H stretch at 3150 cm^{-1}. When deuterated, the O—H stretch shifts down to 2320 cm^{-1} (orange lines in Fig. 3) and the C—H stretch to 2250 cm^{-1} (blue lines in Fig. 3).

To quantitatively describe relative intensities of the infrared bands it would be necessary to go beyond simple point charge models and to use fluctuating charges, multipole models,[41] or a fitted dipole moment surface.[42] However, to locate and approximately assign the fundamentals, the combination of harmonic analysis, calculation of the IR spectrum from the MD simulations with a simplified charge model, and the power spectra are sufficient.

To the best of our knowledge, the IR spectrum of MA in water solution has not been observed as yet. Thus, the predicted solution spectrum for MA and certain features discussed below can serve as a meaningful test for the MMPT force field. With water as a solvent, characteristic shifts (solvatochromic shifts) can be expected, in particular, for modes involving H* due to strong interaction with the oxygen atoms of the water. Indeed, in going from CHO—CH=CH—OH to CHO—CD=CH—OD the OH*O in plane bending shifts by 350 cm^{-1} to the red in vacuum whereas the shift in solution increases to 370 cm^{-1} (see Fig. 4). Similar isotopic shifts for C—H and O—H* stretches are found. Such effects should be observable in experiments. Furthermore, the expected solvent-induced broadening for each band due to the coupling between the solute and solvent degrees of freedom is observed. It is found that C—H bending or stretching modes (green and blue lines) broaden less than the corresponding O—H* modes (red and orange lines). This is reasonable since the O—H*—O hydrogen bonded hydrogen atom couples to the water more strongly than the C—H

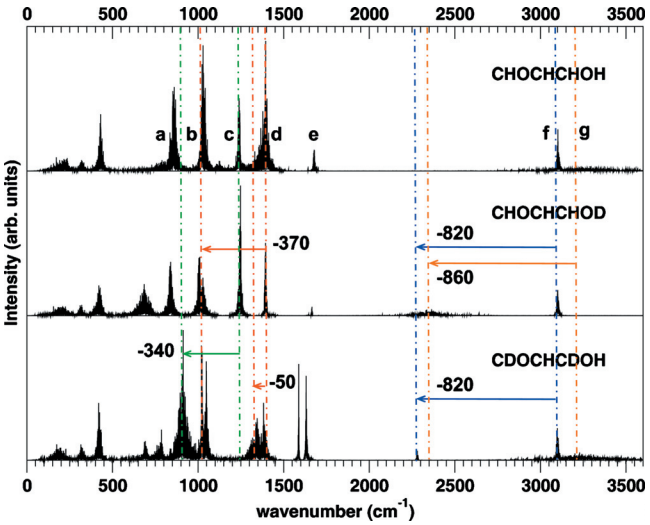

FIG. 4. Infrared spectra of MA and its deuterated isotopomers in solution. From top to bottom are CHO—CH=CH—OH, CHO—CH=CH—OD, and CDO—CH=CD—OH, respectively. The orange, blue, red, and green lines correspond to the O—H* stretch, C—H stretch, O—H*—O in plane bending, and C—H_7+C—H_9 in plane bending, respectively. Bands of particular interest are labeled a-g with detailed assignments in Table I.

bonds due to increased electrostatic interactions. Unlike for other O—H*—O bonded systems, the O···O mode in MA is infrared active since it strongly couples to the OH*···O mode. The relative intensity of the O···O mode [compare Fig. 2(c) with top panel Fig. 4] is considerably reduced in solution compared to the gas phase because the coupling of the OH*···O mode to the O···O mode is smaller. The reason for this is the interaction between the solvent-water molecules and the transferring hydrogen which reduces the coupling.

In conclusion, the MMPT force field was fitted to structural data from *ab initio* calculations and a one-dimensional potential along the bending coordinate *d*. Consequently, the force field correctly captures such properties, as shown in Fig. 1. On the other hand, the MMPT force field was *not* fitted to spectroscopic data for the following reasons: First *ab initio* harmonic frequencies are expected to be less reliable than *ab initio* stationary configurations; second even two qualitatively good PESs may have large deviations of harmonic frequencies [e.g., the RMSD between MP2/6-311++G** and B3LYP/6-31G (often used for larger molecules) frequencies at the minimum is 51 cm^{-1}]; third a spectroscopically accurate force field for MA is beyond the scope of the present work which presents a generalization of MMPT to nonlinear H-bonds. Because frequencies from the MMPT force field were not fitted to *ab initio* calculations, comparison is primarily made between MMPT and experiment. It is found that the calculated spectra from the MD simulations of the three isotopomers agree with existing experimental data[17] with a root mean square deviation (RMSD) between 57 and 83 cm^{-1} for each isotopomer (see the last row of Table I). Large deviations are mainly due to two reasons: first, the O—H*—O bending vibrations are coupled to other modes; second, we assumed the C—H stretch in MA to be threefold degenerate while experimentally this is not the case. Excluding the OH*O bending and the CH stretching vibration leads to a RMSD of 41 cm^{-1} between MMPT/normal modes and experiment for MA (decreased by 42 cm^{-1}). Harmonic frequencies from the MMPT differ from MP2/6-311++G** calculations by 95 cm^{-1} (see Table II in supplementary material). The difference is again dominated by CH- and H*-containing modes. The RMSD between experiment and MP2/6-311++G** calculations is 154 cm^{-1} (with OH* stretch) and 110 cm^{-1} (without OH* stretch) compared to 103 and 73 cm^{-1}, respectively, from harmonic MMPT frequencies. If needed, the differences for the C—H and C=O modes could be reduced by straightforward reparametrization of the force field (see Ref. 39) which was, however, not further pursued in the present work.

C. Estimation of ground state tunneling splitting

The ground state tunneling splitting is also an interesting quantity which has been observed experimentally with very high accuracy. In this section a newly developed HBA Hamiltonian method will be introduced and used to study the ground state splitting in MA.[14,15] The starting point for the formal development is the classical one-dimensional reaction path Hamiltonian derived by Miller and coworkers,[43,44]

$$H(p_s,s,\{P_k,Q_k\}) = \sum_{k=1}^{3N-7}\left(\frac{1}{2}P_k^2+\frac{1}{2}\omega_k^2(s)Q_k^2\right)+V_0(s) + \frac{1}{2}\frac{\left[p_s-\Sigma_{k,l=1}^{3N-7}Q_kP_lB_{k,l}(s)\right]^2}{\left[1+\Sigma_{k=1}^{3N-7}Q_kB_{k,3N-6}(s)\right]^2}, \quad (5)$$

where s is a mass weighted reaction coordinate defined as $s=[\sqrt{m_H}*(R_{O_1H_6}-R_{O_5H_6})]/2$ where m_H is the hydrogen mass and $\{Q_k\}$ are the normal modes orthogonal to s with corresponding conjugate momenta p_s and $\{P_k\}$. The definition of s follows that of Ref. 44 for a RSH which is different from the definition of a reaction path coordinate in Ref. 43. The zeroth order potential $V_0(s)$ is obtained from constrained optimizations with fixed s and the normal mode frequencies $\{\omega_k(s)\}$ from diagonalizing the projected Hessian matrix of the optimized structure where $\{B_{k,l}(s)\}$ are the corresponding coupling parameters as detailed in Ref. 43. According to a very recent study on quantum kinetic energy operators[45] the quantum Hamiltonian can be obtained from Eq. (5) by replacing each P_k^2 by $P_k^\dagger P_k$ and the last term $[p_s-\cdots]^2/[1+\cdots]^2$ by $[p_s-\cdots]^\dagger[1+\cdots]^{-2}[p_s-\cdots]$. In the following the simplified notations P_k^2 and $[p_s-\cdots]^2/[1+\cdots]^2$ are still used to denote $P_k^\dagger P_k$ and $[p_s-\cdots]^\dagger[1+\cdots]^{-2}[p_s-\cdots]$, respectively. According to Ref. 45 each $P_k^\dagger=P_k$ is Hermitian while p_s is non-Hermitian.

The aim of the present development is to find a suitably reduced model which captures the essential elements of the nuclear dynamics and the couplings between the various degrees of freedom rather than solving the full-dimensional Hamiltonian, which has been done elsewhere.[23] First the zeroth order one-dimensional model is considered by ignoring all couplings between the reaction coordinate s and the bath modes $\{Q_k\}$,

$$H_0(p_s,s) = \tfrac{1}{2}p_s^2 + V_0(s).$$

The necessary input data, $V_0(s)$, for evaluating the tun-

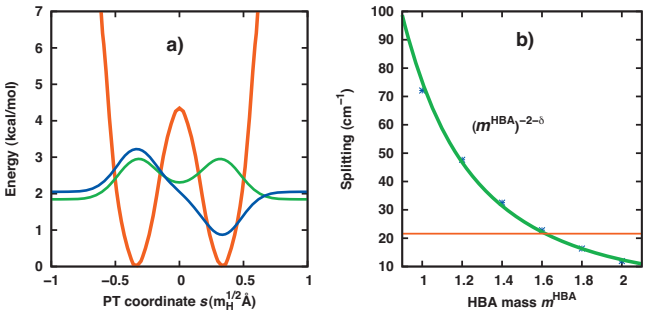

FIG. 5. Ground state tunneling splitting and its parameter dependence. CCSD(T) potential curve $V_0(s)$ calculated at MP2 optimized geometries along the reaction coordinate (a). Also shown are the lowest pair of eigenfunctions. The tunneling splitting as a function of the effective mass m^{HBA} (b).

neling splittings can either be calculated from *ab initio* calculations or from the MMPT potential. A quantitative analysis will first be carried out based on *ab initio* calculations. In a next step the performance of MMPT will be discussed. The potential curve $V_0(s)$ is calculated at the CCSD(T)/6-311++G** level with geometries from MP2/6-311++G** constrained optimizations with fixed s on an equally spaced grid. The barrier height is $\Delta E_b = 4.36$ kcal/mol as already mentioned in Sec. II A. Figure 5(a) shows the calculated potential curve $V_0(s)$ together with the lowest pair of wavefunctions obtained by diagonalization of the zeroth order Hamiltonian H_0. Eigenvalues and eigenvectors for one-dimensional Hamilton operators are obtained by direct diagonalization in a Fourier grid discrete representation in the present work.[46] The difference in the lowest pair of eigenenergies of H_0 gives a ground state tunneling splitting of 72.1 cm^{-1}. This overestimates the experimentally observed splitting by a factor of ~4 and is related to the fact that H_0 is not adequate because important couplings between s and $\{Q_k\}$ are neglected.

In the following the effects of the couplings will be included within the framework of a HBA Hamiltonian. The formal development starts from the following ansatz for the ground state wavefunction of Eq. (5):

$$\Psi(s,\{Q_k\}) = \Phi(s)\prod_{k=1}^{3N-7}\Phi_{\mathrm{HO}}(s,Q_k), \tag{6}$$

where $\Phi_{\mathrm{HO}}(s,Q_k)$ is the ground state wavefunction of the corresponding harmonic oscillator (HO), which parametrically depends on s, namely,

$$\left(\tfrac{1}{2}P_k^2 + \tfrac{1}{2}\omega_k^2(s)Q_k^2\right)\Phi_{\mathrm{HO}}(s,Q_k) = \tfrac{1}{2}\omega_k(s)\Phi_{\mathrm{HO}}(s,Q_k).$$

Calculating the reduced density by integrating out $\{Q_k\}$ on both sides of Eq. (6) one finds that $|\Phi(s)|^2$ is the one-dimensional reduced density along the reaction coordinate s. By averaging Eq. (5) over $\{Q_k\}$ the following one-dimensional HBA Hamiltonian H^{HBA} is obtained:

$$\begin{aligned} H^{\mathrm{HBA}}(p_s,s) &\approx \left\langle \prod_{k=1}^{3N-7}\Phi_{\mathrm{HO}}(s,Q_k)\middle|\sum_{k=1}^{3N-7}\left(\frac{1}{2}P_k^2+\frac{1}{2}\omega_k^2(s)Q_k^2\right)\middle|\prod_{k=1}^{3N-7}\Phi_{\mathrm{HO}}(s,Q_k)\right\rangle + V_0(s) \\ &\quad + \frac{1}{2}\frac{\left\langle \Pi_{k=1}^{3N-7}\Phi_{\mathrm{HO}}(s,Q_k)\middle|\left[p_s - \Sigma_{k,l=1}^{3N-7}Q_kP_lB_{k,l}(s)\right]^2\middle|\Pi_{k=1}^{3N-7}\Phi_{\mathrm{HO}}(s,Q_k)\right\rangle}{\left\langle \Pi_{k=1}^{3N-7}\Phi_{\mathrm{HO}}(s,Q_k)\middle|\left[1+\Sigma_{k=1}^{3N-7}Q_kB_{k,3N-6}(s)\right]^2\middle|\Pi_{k=1}^{3N-7}\Phi_{\mathrm{HO}}(s,Q_k)\right\rangle} \\ &= \frac{1}{2}\frac{p_s^2}{1+\Delta_s} + V_0(s) + \sum_{k=1}^{3N-7}\frac{\omega_k(s)}{2}\left(1+\frac{\Delta_k}{1+\Delta_s}\right), \end{aligned} \tag{7}$$

which includes important contributions of both kinetic and potential couplings and $\Delta_s(s)=\Sigma_k|B_{k,3N-6}(s)|^2/2\omega_k(s)$ and $\Delta_k(s)=\Sigma_l|B_{l,k}(s)|^2/2\omega_l(s)$ are both non- negative functions. Here the average of the last term $[p_s-\cdots]^2/[1+\cdots]^2$ in Eq. (5) is approximated by $\langle[p_s-\cdots]^2\rangle/\langle[1+\cdots]^2\rangle$ since correlations are only fourth order quantities of the coupling parameters $\{B_{k,l}(s)\}$. The term $p_s^2/(1+\Delta_s)$ actually should be evaluated as $p_s\dagger(1+\Delta_s)^{-1}p_s$ as mentioned above. Thus, $H^{\mathrm{HBA}}(p_s,s)$ is a well defined operator without singularity or large curvature problems irrespective of whether it is one- or multidimensional[44] compared to other reduced models based on reaction path/surface Hamiltonians. The HBA Hamiltonian manifestly includes the effects of the bath modes and is thus expected to more realistically describe the dynamics of a multidimensional system. A closer inspection of $H^{\mathrm{HBA}}(p_s,s)$ reveals that it contains two modifications compared to H_0, which can be conveniently expressed as

$$m^{\mathrm{HBA}}(s) = 1+\Delta_s \tag{8}$$

which plays the role of an effective mass instead of 1 due to kinetic couplings, and an effective potential

$$V^{\mathrm{HBA}}(s) = V_0(s) + \sum_{k=1}^{3N-7}\frac{\omega_k(s)}{2}\left(1+\frac{\Delta_k}{1+\Delta_s}\right). \tag{9}$$

Note that by working with H^{HBA} one is no longer treating the original H* atom but a different "particle" which involves additional contributions due to coupling to the bath modes. As a result there is a different effective mass and effective potential for the new particle. One can readily see that H^{HBA} involves a mass function $m^{\mathrm{HBA}}(s)>1$ and an effective barrier $\Delta E_b^{\mathrm{HBA}}(V^{\mathrm{HBA}})>\Delta E_b(V_0)$, which both will lead to reduced tunneling splittings.

In principle, the two essential quantities $m^{\mathrm{HBA}}(s)$ and $V^{\mathrm{HBA}}(s)$ can be calculated from either *ab initio* information or from the force field according to Eqs. (8) and (9) and the definition of the coupling parameters $\{B_{k,l}(s)\}$, which characterize the variation of eigenvectors of bath modes along the reaction path.[43] The detailed procedures to compute $m^{\mathrm{HBA}}(s)$ and $V^{\mathrm{HBA}}(s)$ according to Eqs. (8) and (9) have been given previously.[43] A full analysis of H^{HBA} including the comparison of $m^{\mathrm{HBA}}(s)$ and its full-dimensional equivalent will be discussed in separate work. Here an alternative route is pursued because experimental data for both HT and deuterium transfer (DT) are available (see below). It is instructive to first consider how the tunneling splitting depends parametrically on $m^{\mathrm{HBA}}(s)$. Figure 5(b) shows the ground state tunneling splitting as a function of the effective mass m^{HBA} with the zeroth order barrier ΔE_b=4.36 kcal/mol, i.e., the zero order potential $V_0(s)$. Here $m^{\mathrm{HBA}} \approx \langle m^{\mathrm{HBA}}(s) \rangle$ is used for simplicity instead of $m^{\mathrm{HBA}}(s)=1+\Delta_s$ (more precisely m^{HBA} is defined through the relation $\langle p_s^2 \rangle / m^{\mathrm{HBA}} = \langle p_s^2 / m^{\mathrm{HBA}}(s) \rangle$). The result can be represented as a decaying function $(m^{\mathrm{HBA}})^{-2-\delta}$ with δ=0.6, as shown in Fig. 5(b). As can be seen the tunneling splitting decreases with increasing effective mass.

Equation (7) establishes that $V^{\mathrm{HBA}}(s)$ and consequently $\Delta E_b^{\mathrm{HBA}}$ can be estimated by including all zero point energies of the $3N-7$ bath modes for each grid point, which then corresponds to the commonly used model potential[47] of reduced dimensionality models with $\Delta_k=0$ for each bath mode. Based on the harmonic analysis of the global minimum and the TS structure, the total zero point energy changes in the bath modes leads to 2.33 kcal/mol increase of the HBA barrier height $\Delta E_b^{\mathrm{HBA}}$, which agrees well with the value reported in Ref. 47 and the harmonic frequencies from Ref. 25. Therefore, the zero point energy corrected HBA barrier at the present CCSD(T)/6-311++G** level with the MP2 geometries is E_b^{HBA}=6.7 kcal/mol, which is used for further calculations.

To determine m^{HBA}, the tunneling splittings for the hydrogenated and the deuterated systems are considered. Experimental splittings for H*- and D*-tunneling are 21.583 and 2.915 cm^{-1}, respectively.[14,15,48] Computationally, the reaction coordinates for H*- and D*-transfers are $s=\frac{1}{2}\sqrt{m_{\mathrm{x}}}(R_{\mathrm{O_1X_6}}-R_{\mathrm{O_5X_6}})$ with X=H or D and the underlying potential $V_0(s)$ for H*- and D*-transfers in MA is identical, except that the mass weighted coordinate is scaled by $\sqrt{m_{\mathrm{D}}/m_{\mathrm{H}}}$ for D*-transfer. According to Ref. 43 the coupling parameters $B_{k,l}(s)$ are matrix elements of $\partial/\partial s$ and $\propto\sqrt{1/m_{\mathrm{H}}}$ for hydrogenated MA and $\propto\sqrt{1/m_{\mathrm{D}}}$ for deuterated MA. From this the relationship $\Delta_s^D/\Delta_s^H=m_H/m_D$ can be derived. Therefore, the correction (compared to the uncoupled model H_0) to m^{HBA} for D* transfer is half of that for H* transfer. Consequently, for the given HBA barrier ΔE^{HBA}=6.7 kcal/mol, there are two experimentally measured splittings and one free parameter ($m_{\mathrm{H*}}^{\mathrm{HBA}}$) in the computational model, which allows us to test and validate the theoretical model. For a H*-tunneling splitting of 21.6 cm^{-1}, Δ_s^{H}=0.234 and $m_{\mathrm{H*}}^{\mathrm{HBA}}$=1.234. Using $\Delta_s^{\mathrm{D}}/\Delta_s^{\mathrm{H}}=m_{\mathrm{H}}/m_{\mathrm{D}}$ gives $m_{\mathrm{D*}}^{\mathrm{HBA}}$=1.117 from which the calculated splitting for D*-tunneling is 2.8 cm^{-1}, in very good agreement with experiment. Using these parameters ($m_{\mathrm{H*}}^{\mathrm{HBA}}$=1.234, $m_{\mathrm{D*}}^{\mathrm{HBA}}$=1.117, and $\Delta E_b^{\mathrm{HBA}}$=6.7 kcal/mol), it is also possible to calculate the infrared active H* transfer and D* transfer fundamental excitations. With $|\nu p\rangle$ to label the state, where ν is the vibrational quantum number and p is the parity, for H* transfer the $|1-\rangle \leftarrow |0+\rangle$ transition is found at 1573 cm^{-1} and the $|1+\rangle \leftarrow |0-\rangle$ at 1267 cm^{-1}, respectively. The ground state is $|0+\rangle$. Replacing hydrogen by deuterium leads to fundamental transitions at 1136 and 1068 cm^{-1}, respectively.

It is also possible to compute all necessary data for the HBA Hamiltonian from the MMPT potential. The barrier of $V_0(s)$ obtained by CHARMM/MMPT optimizations is ΔE_b=4.3 kcal/mol, which agrees quite well with the above CCSD(T)/6-311++G** value at the MP2/6-311++G** geometries and also agrees with 4.1 kcal/mol reported by Bowman group from CCSD(T)/aug-cc-pV5Z PES.[25] Using the harmonic frequencies from the MMPT potential leads to a zero point energy corrected HBA barrier height $\Delta E_b^{\mathrm{HBA}}$=5.1 kcal/mol. With the same effective mass $m_{\mathrm{H*}}^{\mathrm{HBA}}$=1.234 a splitting of 36.1 cm^{-1} for H* tunneling is obtained. The pairs of infrared active O—H* stretch fundamental transitions are 1417 and 1036 cm^{-1}, respectively. For D* transfer the tunneling splitting amounts to 5.8 cm^{-1} and the two O—D* stretch fundamentals are at 999 and 887 cm^{-1}, respectively. Given the simplicity and drastically reduced computational effort for the MMPT force field, such agreement is acceptable.

D. Hydrogen transfer rates of MA

Apart from the infrared spectra and ground state tunneling splitting which have been extensively investigated both experimentally and theoretically, the MMPT potential can also be used to study the HT rate. This is also of interest in view of previous *ab initio* molecular dynamics simulations (see Sec. IV) that studied the over-the-barrier process.[49] In the following a classical dynamics approach is used which provides lower limits for H-transfer rates. To include quantum effects, flux-flux autocorrelation functions are required which is computationally very expensive and beyond the purpose of the present work.[50] First the classical rate, i.e., the incoherent over-the-barrier (hopping) process, is considered while the quantum mechanical nature of gas phase H-transfer will be discussed below. As has been mentioned in Sec. II B the hydrogen hopping rate is calculated from the slope of hazard plots, which is straightforward from MD simulations.

The classical hydrogen hopping rates of MA with different barrier heights are shown in Fig. 6(a). The three curves correspond to barrier heights of 3.4, 1.7, and 0.9 kcal/mol, respectively. The corresponding HT rates are 7/ns, 37/ns, and 410/ns, respectively. An approximately exponential decay of the hopping rate with increasing barrier height can be found in Fig. 6(a), which is reasonable when only classical hopping is involved. Apart from the HT rate which characterizes the statistically averaged behavior, various rapid processes (with lifetime on the femtosecond time scale) are found from the hazard plots. They reflect the complicated dynamics of the entire system. The rates of these fast processes are primarily

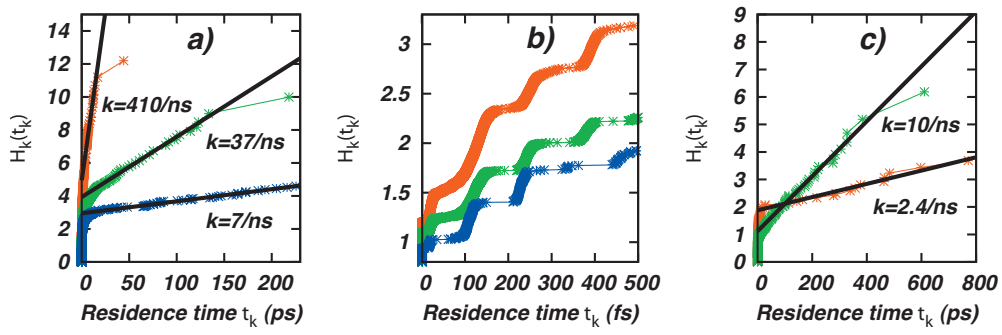

FIG. 6. Hydrogen hopping rates of MA with different barrier heights in vacuum (a). Direct hydrogen hopping rates of MA with different barrier heights in vacuum (b). Hydrogen hopping rates of MA in vacuum (red) and solution (green) (c). For (a) and (b) the barrier heights for the red, green, and blue curves are 3.4, 1.7, and 0.9 kcal/mol, respectively.

determined by the period of the motions around the minimum configurations and consequently do not depend appreciably on the barrier height. As an example, only the rapid processes are shown in Fig. 6(b), which is an enlarged part of Fig. 6(a) for times $t<500$ fs. The fastest process is a direct HT with large velocity between D and A, which is completed in less then 1 fs. A lower barrier leads to a larger number of direct transfers. The second fastest process is the transfer from D (or A) to A (or D) after one vibrational period in the local potential well (one period is $\approx$10 fs for a harmonic frequency of 3000 cm^{-1}). Due to the anharmonicity of the PES and the couplings with other modes, the rate of this process is much slower than the harmonic frequency of the O—H mode. Typical rates are around 15/ps and depend primarily on the curvature of the PES around the minimum and the coupling between different degrees of freedom. Several of such processes can be found in Fig. 6(b) with different residence times.

Figure 6(c) shows the hydrogen hopping rates from classical MD simulations in vacuum and solution, respectively, using the MMPT potential with a barrier height of 4.3 kcal/mol. The solvent significantly enhances the hopping rate of the hydrogen from 2.4/ns to 10/ns. This implies a strong coupling between the transferring hydrogen and the solvent water, which is consistent with the above mentioned spectra in solution. For the rapid processes fewer direct transfers are found in solution compared to vacuum due to the increased density of states.

So far only the incoherent, over-the-barrier process has been discussed for both MA in gas and condensed phase. In reality, H-transfer for MA in the gas phase and at low to ambient temperatures is dominated by the coherent process (tunneling) due to the much lower density of states. For discussing the tunneling process, the low temperature limit is considered which is also approximately valid for higher temperatures given the fact that even at room temperature, the available thermal energy ($\approx$200 cm^{-1}) is not sufficient to significantly populate vibrationally excited states. The evolution of the system at low temperature is characterized by the time-dependent quantum state

$$|\Psi(t)\rangle = e^{-iE_{0+}t}(C_+|0+\rangle + C_-e^{-i\Delta_0 t}|0-\rangle).$$

Here C_+ and C_- are (in general complex-valued) expansion coefficients of the initial state $|\Psi(0)\rangle = C_+|0+\rangle + C_-|0-\rangle$ and $\Delta_0 = E_{0-} - E_{0+}$ is the tunneling splitting reported in the previous section. With $|\Phi_{L/R}\rangle = (|0+\rangle \pm |0-\rangle)/\sqrt{2}$ [left (L) and right (R) localized states according to the one-dimensional wavefunctions associated with $|0\pm\rangle$; see Fig. 5(a)], the time-dependent probability for finding the proton in the left or right potential well is $P_{L/R}(t) = |\langle\Psi(t)|\Phi_{L,R}\rangle|^2$. From this the time evolution of the probability difference between L and R is

$$\Delta P_{LR}(t) = P_L(t) - P_R(t) = \Delta P_{\max}\cos(\Delta_0 t + \phi_0).$$

Here, $\Delta P_{\max}$ is the amplitude of the oscillation and the phase ϕ_0 is the difference between the arguments of the initial expansion coefficients C_+ and C_- (which will vanish if both coefficients are real). The equation for $\Delta P_{LR}(t)$ gives rise to a tunneling frequency ω associated with $\Delta_0 = 21.6$ cm^{-1} $= 648/\text{ns} \approx 1/\text{ps}$. The significantly higher tunneling frequency compared to the 2.4/ns hopping rate from MD simulations also clearly shows the coherent nature of H-transfer in the gas phase. Experimentally, this process is characterized by a tunneling frequency (splitting) and not by a rate constant.

IV. DISCUSSION AND CONCLUSIONS

The present work presents a generalized MMPT reactive force field to characterize PT in both linear and nonlinear hydrogen bonds. To obtain a robust parametrization to describe H^* transfer in complex systems, two pairs of parameters (force constant and equilibrium displacement around the minimum and transition state configurations) have to be fit and the PES is subjected to morphing transformations to reflect the corresponding chemical environment. This force field has been applied to MA to investigate the intramolecular nonlinear hydrogen bond. With this PES it is possible to calculate meaningful structures and qualitatively correct infrared spectra for MA without fitting to experimental data. Further refinements will be possible but are outside the scope of the present work. The tunneling splittings for HT and DT were also calculated based on a newly developed HBA Hamiltonian, which is characterized by a larger effective mass and an increased barrier, both of which are results of couplings to the bath modes. Using data from *ab initio* calculations and the parametrized MMPT potential, close agreement of the tunneling splittings with experiment is found for

both HT and DT. A more detailed future discussion of the HBA Hamiltonian should also lead to additional insight.

The spectra were assigned by exploring isotope effects and power spectra corresponding to particularly relevant internal coordinates. The calculated gas phase infrared spectra agree with experiments for all isotopomers investigated in this work. Spectra of MA in solution have also been predicted and it will be interesting to compare them with forthcoming experiments. The C—H in- and out-of-plane bending and the C—H stretch vibrations have been found to broaden less than the O—H* bending or stretch vibrations for solvated MA due to less strong coupling between the C—H bond and the water than the one between the O—H* and water. The effective HBA particle defined by the HBA Hamiltonian has been found to have a larger effective mass and a higher effective barrier to tunnel through than the particle in an uncoupled model. Both effects will lead to reductions of the splitting previously obtained from uncoupled models. An H* tunneling splitting of 21.6 cm^{-1} (2.8 cm^{-1} for D*) and O—H* stretch fundamental of 1573 cm^{-1} (1136 cm^{-1} for O—D* stretch) have been obtained from an effective HBA barrier $\Delta E_b^{\mathrm{HBA}}=6.7$ kcal/mol and an effective mass $m_{\mathrm{H}*}^{\mathrm{HBA}}=1.234$ ($m_{\mathrm{D}*}^{\mathrm{HBA}}=1.117$ for D*), which agrees well with previous investigations. For the classical hydrogen hopping processes both direct (nonobservable, femtosecond time scale) and averaged (observable, ps time scale) rates have been studied. The water solvent has been found to play an important role for the HT in solution, which actually enhanced the hopping rate by a factor of 4 compared to that in vacuum.

The HBA Hamiltonian in Eq. (7) provides a meaningful explanation for the observed ground state tunneling splitting in MA. It is straightforward to generalize Eq. (7) for multidimensional reduced HBA Hamiltonians starting from a RSH using the same techniques. An attractive feature of H^{HBA} is the limited computational effort that is required to describe quantum effects such as tunneling splittings and zero point vibrations in fairly large molecules. The present treatment finds a splitting of 72.1 cm^{-1} from a one-dimensional uncoupled model H_0, which is reduced to 21.6 cm^{-1} by including both kinetic and potential couplings between s (reaction coordinate) and Q_k (bath modes). The reduction of the splitting when including the couplings has already been previously reported.[23] There, a splitting of 51 cm^{-1} was obtained from a two dimensional uncoupled model compared to a splitting of 11 cm^{-1} from a full-dimensional RSH using a MP2/6-31G** PES. By including higher than second order terms in the analytical representation of the PES, the tunneling splitting increases to 15 cm^{-1}. A more recent study using an extensive number of points calculated at the CCSD(T) level with extrapolation to the near-basis set limit reports a tunneling splitting of 21–22 cm^{-1} depending on how the coordinates are treated.[25] The barrier for H-atom transfer is found to be 4.1 kcal/mol, which is close to the value of 4.3 kcal/mol found on the present MMPT surface. Earlier work has found barriers of 3.6 kcal/mol and corresponding tunneling splittings of 13.9 cm^{-1} by employing MP2/6-31G(d,p) for the PES and classical dynamics simulations from which tunneling splittings were estimated by using semiclassical theory.[51,52] In another, related study, a modified spectroscopic force field derived from early experimental studies of MA (Refs. 14, 17, and 53) was used together with classical dynamics simulations and semiclassical theory to calculate tunneling splittings. The PES had a barrier for HT of 10 kcal/mol and the calculated tunneling splittings were 21.8 cm^{-1}, in very good agreement with experiment. Finally, using semiclassical wave packet calculations in reduced dimensionality, splittings of 21 cm^{-1} were found with a potential energy barrier of 2.3 kcal/mol.[54] According to the present investigation, some previously reduced dimensional studies will probably fail to give quantitative results for D* tunneling splitting unless a different potential barrier from that for H* tunneling is used. These comparisons suggest that using high-level *ab initio* calculations for the PES together with reliable procedures to describe the nuclear dynamics converge to barrier heights for H-transfer of ≈4 kcal/mol, which lead to tunneling splittings of ≈22 cm^{-1}. Using the MMPT potential validated in this fashion leads to a H-transfer mode at 1573 cm^{-1} by using the HBA Hamiltonian, which is supported by the finding of a low frequency O—H* stretch mode (1672 cm^{-1}) from a full-dimensional RSH.[23]

The calculated H-transfer rate of 10/ns in solution qualitatively agrees with previous investigations.[49,55] Starting from a diffusion equation, a recent computational study obtained rates of 38/ns for the H-transfer rate and slightly lower barriers for the transfer in solution compared to vacuum.[55] On the other hand, *ab initio* MD simulations of MA in water have been carried out with self consistent charges density functional tight binding (SCC-DFTB).[49] This study finds a long rate constant of 29/ns, qualitatively similar to the rate found here, and two rapid processes (6/ps and 100/ps), which correspond to the rapid processes in Fig. 6(b). To the best of our knowledge, the only experimental estimate characterization of the energetics comes from NMR studies in $CFCl_3$ and CD_2Cl_2, which find an upper limit of 6 kcal/mol for the HT reaction.[56]

It is also interesting to compare the vibrational spectroscopy of the HT stretch band for MA with the spectroscopy of other proton-bound complexes. For weakly bonded systems (such as He—HCO^+ or He—HN_2^+) (Refs. 57 and 58) the vibrational redshifts of the ν_1 hydrogen stretch are only −12.4 and −75 cm^{-1}, which reflect the small perturbation caused by a helium atom in the H* stretch motion. Contrary to that, complexation with Ar leads to substantial shifts of −274 and −728.5 cm^{-1}, respectively.[59,60] Considering the spectroscopic data gathered so far on Rg-HCO^+ and Rg-HN_2^+ complexes (Rg=He,Ne,Ar) it was observed that the vibrational redshift of the ν_1 stretch correlates linearly with the difference in proton affinity ΔPA between the rare gas atom and the CO or N_2 moiety, respectively.[61] These relationships are also reflected in the strength of the hydrogen bond between the Rg atom and the ionic core, which range between 1 and 8 kcal/mol for He- and Ar—HN_2^+.[62,63] Contrary to that, the proton stretch fundamental in more strongly bonded protonated water (H_2O—H^+—OH_2) or ammonia (H_3N—H^+—NH_3) dimers with hydrogen bond energies larger than 20 kcal/mol are expected to shift even more to the red. For H_3O^+ the totally symmetric OH stretch ν_1 consists

of two components ν_1^+ and ν_1^- with origins at 3390 and 3491 cm^{-1}, respectively.[64] Complexation with another water molecule shifts this frequency by more than -2000 cm^{-1} to the red.[4,7] Similarly, the $N—H^*$ stretch mode in NH_4^+ is also greatly shifted to the red by more than -2000 cm^{-1} when bonded with another ammonia molecule.[21] For MA the hydrogen bond energy was estimated by comparing the energy difference between the enol and *trans* conformers, which amounts to ≈12 kcal/mol at the MP2/6-311+G** level. This is between that of $Ar—HN_2^+$ and $H_2O—H^+—OH_2$. Consequently, the $O—H^*$ stretch in MA is expected to shift to the red by more than -1000 cm^{-1}, which is supported by the present work (1573 cm^{-1}) and other recent investigations (1672 cm^{-1}).[23] It should, however, be noted that the "hydrogen bond energy" in protonated complexes and MA are likely to differ slightly in their chemical meanings as it is an intramolecular H-bond in MA and intermolecular H-bonds in all other systems mentioned.

In conclusion, the present work has extended MMPT to nonlinear hydrogen bonds which will be particularly useful for studying biomolecular systems. The parametrization has been validated for MA by comparing with vibrational spectroscopic and tunneling data available from experiments, structures, and barriers from high-level *ab initio* calculations. After including zero point corrections to the barrier for HT due to the bath modes, an increased effective mass of the transferring particle (compared to the uncoupled model) has been found to yield a splitting of the vibrational ground state in good agreement with experiment. Based on preliminary calculations with a HBA Hamiltonian the HT stretch mode is most likely located around 1600 cm^{-1}, which is in agreement with other recent computational work[23] but at variance with assignments from experiment. A redshift of more than -1000 cm^{-1} of the $OH^*—O$ stretch mode is also expected from analogies with other proton-bound systems, which are consistent with the suggestion in Ref. 23 that previous assignments may be incorrect.

ACKNOWLEDGMENTS

This work was supported by the Schweizerischer Nationalfonds under Grant No. 200021-117810.

[1] C. J. T. de Grotthuss, Ann. Chim. **LVIII**, 54 (1806).
[2] *Hydrogen-Transfer Reactions*, edited by J. T. Hynes, J. P. Klinman, H.-H. Limbach, and R. L. Schowen (Wiley-VCH, Weinheim, 2007).
[3] K. R. Asmis, N. L. Pivonka, G. Santambrogio, M. Brümmer, C. Kaposta, D. M. Neumark, and L. Wöste, Science **299**, 1375 (2003).
[4] E. Diken, J. Headrick, J. Roscioli, J. Bopp, M. A. Johnson, and A. McCoy, J. Phys. Chem. A **109**, 1487 (2005).
[5] K. R. Asmis, Y. Yang, G. Santambrogio, M. Brümmer, J. R. Roscioli, L. R. McCunn, M. A. Johnson, and O. Kühn, Angew. Chem., Int. Ed. **46**, 8691 (2007).
[6] K. Giese, M. Petković, H. Naundorf, and O. Kühn, Phys. Rep. **430**, 211 (2006).
[7] O. Vendrell, F. Gatti, and H. D. Meyer, Angew. Chem., Int. Ed. **46**, 6918 (2007).
[8] A. B. McCoy, X. Huang, S. Carter, and J. M. Bowman, J. Chem. Phys. **123**, 064317 (2005).
[9] Y. Yang and O. Kühn, Z. Phys. Chem. **222**, 1375 (2008).
[10] M. Meuwly and M. Karplus, J. Chem. Phys. **116**, 2572 (2002).
[11] V. Zoete and M. Meuwly, J. Chem. Phys. **120**, 7085 (2004).
[12] S. Lammers and M. Meuwly, J. Phys. Chem. A **111**, 1638 (2007).
[13] S. Lammers, S. Lutz, and M. Meuwly, J. Comput. Chem. **29**, 1048 (2008).
[14] S. L. Baughcum, R. W. Duerst, W. F. Rowe, Z. Smith, and E. B. Wilson, J. Am. Chem. Soc. **103**, 6296 (1981).
[15] D. W. Firth, K. Beyer, M. A. Dvorak, S. W. Reeve, A. Grushow, and K. R. Leopold, J. Chem. Phys. **94**, 1812 (1991).
[16] C. J. Seliskar and R. E. Hoffmann, J. Mol. Spectrosc. **96**, 146 (1982).
[17] Z. Smith and E. B. Wilson, Spectrochim. Acta, Part A **39**, 1117 (1983).
[18] D. W. Firth, P. F. Barbara, and H. P. Trommsdorf, Chem. Phys. **136**, 349 (1989).
[19] T. Chiavassa, R. Roubin, L. Piazzala, P. Verlaque, A. Allouche, and F. Marinelli, J. Phys. Chem. **96**, 10659 (1992).
[20] C. Duan and D. Luckhaus, Chem. Phys. Lett. **391**, 129 (2004).
[21] Y. Yang, O. Kühn, G. Santambrogio, D. J. Goebbert, and K. R. Asmis, J. Chem. Phys. **129**, 224302 (2008).
[22] A. Alparone and S. Millefiori, Chem. Phys. **290**, 15 (2003).
[23] D. P. Tew, N. C. Handy, and S. Carter, J. Chem. Phys. **125**, 084313 (2006).
[24] A. Viel, M. D. Coutinho-Neto, and U. Manthe, J. Chem. Phys. **126**, 024308 (2007).
[25] Y. Wang, B. J. Braams, J. M. Bowman, S. Carter, and D. P. Tew, J. Chem. Phys. **128**, 224314 (2008).
[26] A. Hazra, J. H. Skone, and S. Hammes-Schiffer, J. Chem. Phys. **130**, 054108 (2009).
[27] M. J. Frisch, G. W. Trucks, H. B. Schlegel *et al.*, GAUSSIAN 03, Revision B.04. Gaussian Inc., Wallingford, CT, 2004.
[28] M. Meuwly and J. M. Hutson, J. Chem. Phys. **110**, 8338 (1999).
[29] B. Gazdy and J. M. Bowman, J. Chem. Phys. **95**, 6309 (1991).
[30] B. R. Brooks, R. E. Bruccoleri, B. D. Olafson, D. J. States, S. Swaminathan, and M. Karplus, J. Comput. Chem. **4**, 187 (1983).
[31] W. L. Jorgensen, J. Chandrasekhar, J. D. Madura, R. W. Impey, and M. L. Klein, J. Chem. Phys. **79**, 926 (1983).
[32] J.-P. Ryckaert, G. Ciccotti, and H. J. C. Berendsen, J. Comput. Phys. **23**, 327 (1977).
[33] P. Steinbach and B. Brooks, J. Comput. Chem. **15**, 667 (1994).
[34] M. Schmitz and P. Tavan, J. Chem. Phys. **121**, 12233 (2004).
[35] M. Schmitz and P. Tavan, J. Chem. Phys. **121**, 12247 (2004).
[36] F. J. Harris, Proc. IEEE **66**, 51 (1978).
[37] E. Helfand, J. Chem. Phys. **69**, 1010 (1978).
[38] A. D. MacKerell, D. Bashford, M. Bellott, R. L. Dunbrack, J. D. Evanseck, M. J. Field, S. Fischer, J. Gao, H. Guo, S. Ha, D. Joseph-McCarthy, L. Kuchnir, K. Kuczera, F. T. K. Lau, C. Mattos, S. Michnick, T. Ngo, D. T. Nguyen, B. Prodhom, W. E. Reiher, B. Roux, M. Schlenkrich, J. C. Smith, R. Stote, J. Straub, M. Watanabe, J. Wiorkiewicz-Kuczera, D. Yin, and M. Karplus, J. Phys. Chem. B **102**, 3586 (1998).
[39] See supplementary material at http://dx.doi.org/10.1063/1.3447701 for force field parameters and additional frequency tables.
[40] M. Devereus and M. Meuwly, J. Chem. Inf. Model. **50**, 349 (2010).
[41] N. Plattner and M. Meuwly, Biophys. J. **94**, 2505 (2008).
[42] X. Huang, B. J. Braams, and J. M. Bowman, J. Chem. Phys. **122**, 044308 (2005).
[43] W. H. Miller, N. C. Handy, and J. E. Adams, J. Chem. Phys. **72**, 99 (1980).
[44] T. Carrington and W. H. Miller, J. Chem. Phys. **81**, 3942 (1984).
[45] Y. Yang and O. Kühn, Mol. Phys. **106**, 2445 (2008).
[46] C. Marston and G. Balint-Kurti, J. Chem. Phys. **91**, 3571 (1989).
[47] T. Carrington and W. H. Miller, J. Chem. Phys. **84**, 4364 (1986).
[48] S. L. Baughcum, Z. Smith, E. B. Wilson, and R. W. Duerst, J. Am. Chem. Soc. **106**, 2260 (1984).
[49] L. Walewski, P. Bala, M. Elstner, T. Frauenheim, and B. Lesyng, Chem. Phys. Lett. **397**, 451 (2004).
[50] W. H. Miller, J. Chem. Phys. **61**, 1823 (1974).
[51] K. Yagi, T. Taketsugu, and K. Hirao, J. Chem. Phys. **115**, 10647 (2001).
[52] N. Makri and W. H. Miller, J. Chem. Phys. **91**, 4026 (1989).
[53] T. D. Sewell, Y. Guo, and D. L. Thompson, J. Chem. Phys. **103**, 8557 (1995).
[54] M. Ben-Nun and T. J. Martinez, J. Phys. Chem. A **103**, 6055 (1999).
[55] M. Aschi, M. D'Abramo, F. Ramondo, I. Daidone, M. D'Alessandro, A. D. Nola, and A. Amadei, J. Phys. Org. Chem. **19**, 518 (2006).
[56] R. S. Brown, A. Tse, T. Nakashima, and R. C. Haddon, J. Am. Chem. Soc. **101**, 3157 (1979).
[57] S. A. Nizkorodov, J. P. Maier, and E. J. Bieske, J. Chem. Phys. **103**, 1297 (1995).
[58] M. Meuwly, S. A. Nizkorodov, J. P. Maier, and E. J. Bieske, J. Chem. Phys. **104**, 3876 (1996).

[59] S. A. Nizkorodov, O. Dopfer, T. Ruchti, M. Meuwly, J. P. Maier, and E. J. Bieske, J. Phys. Chem. **99**, 17118 (1995).
[60] S. A. Nizkorodov, Y. Spinelli, E. J. Bieske, J. P. Maier, and O. Dopfer, Chem. Phys. Lett. **265**, 303 (1997).
[61] E. J. Bieske and O. Dopfer, Chem. Rev. (Washington, D.C.) **100**, 3963 (2000).
[62] M. Meuwly and R. J. Bemish, J. Chem. Phys. **106**, 8672 (1997).
[63] O. Dopfer, R. V. Olkhov, and J. P. Maier, J. Phys. Chem. A **103**, 2982 (1999).
[64] J. Tang and T. Oka, J. Mol. Spectrosc. **196**, 120 (1999).